Dry deposition of reactive nitrogen from satellite observations of ammonia and nitrogen dioxide over North America

S. K. Kharol[1]*, M. W. Shephard[1], C. A. McLinden[1], L. Zhang[1], C. E. Sioris[1], J. M. O'Brien[1], R. Vet[1], K. E. Cady-Pereira[2], J. Siemons[1,3], and N. A. Krotkov[4]

[1] Environment and Climate Change Canada, Toronto, Ontario M3H 5T4, Canada.

[2]Atmospheric and Environmental Research, Inc., Lexington, MA, USA.

[3]University of Waterloo, Waterloo, ON, Canada

[4]Atmospheric Chemistry and Dynamics Laboratory, NASA Goddard Space Flight Center, Greenbelt, Maryland, USA

Corresponding author: Shailesh Kumar Kharol (shailesh.kharol@canada.ca; shaileshan2000@gmail.com)

Key Points:

- First use of satellite observations to estimate the dry deposition of reactive nitrogen (N_r) from ammonia (NH_3).
- Satellite estimates of NH_3 and NO_2 dry deposition indicates that the NH_3 dominates over most regions across the North America during the 2013 warm season.
- Locations at northern latitudes affected by forest fires tend to have 2-3 times more dry deposition of ammonia relative to the local background.

Abstract

Reactive nitrogen (N_r) is an essential nutrient to plants and a limiting element for growth in many ecosystems, but can have harmful effects on ecosystems when in excess. Satellite-derived surface observations are used together with a dry deposition scheme to estimate the deposition flux of short-lived nitrogen species, NH_3 and NO_2, over North America during the 2013 warm season. These fluxes demonstrate that the NH_3 contribution dominates over NO_2 for most regions (comprising ~80% of their sum in Canada, and ~65% in US), with some regional exceptions (e.g. Alberta and northeastern-US). Nationwide, ~53 tonnes(N) of these species were dry deposited in the US, more than double the ~23 tonnes(N) in Canada over this period. Forest fires are shown to be the major contributors of dry deposition of N_r from NH_3 in northern latitudes, and can often lead to deposition fluxes 2-3 times more than from expected background amounts without fires.

1. Introduction

Nitrogen (N) is an essential element for the growth and reproduction of plants and animals. While it is the most abundant gas in our atmosphere (78%), it primarily exists in its chemically unreactive form (N_2) that is not usable by most organisms and plants [*Erisman et al.*, 2011]. In order for N to be used by animals and plants it needs to go through the nitrogen fixation process which converts it into reactive nitrogen (N_r), its biologically functional form. N_r is produced naturally through biological nitrogen fixation (i.e., by legumes, blue-green algae, etc.), biomass burning and by lightning. Human activities also lead to nitrogen fixation through production of nitrogen-based fertilizers (e.g. Haber-Bosch industrial production of ammonia) and from the burning of fossil fuels, which changes N to N_r. Presently human-induced exceeds natural fixation [*Fowler et al.*, 2013, 2015], and can dramatically alter the global nitrogen cycle [*Erisman et al*., 2015]. Deposition of N_r into the ecosystem provides important nutrients (e.g., increases crop production), but excessive deposition can cause various deleterious effects on the environment leading to ecosystem impacts such as soil acidification [*Galloway et al.*, 2003], eutrophication [*Bergstrom et al*., 2006], changes to vegetation type, and biodiversity loss [*Fenn et al.*, 2010; *Bowman et al*., 2012; *Sheppard et al*. 2011; *Bauer et al*., 2016].

Implementation of stricter pollution controls to reduce atmospheric emissions from power plants and vehicles have resulted in a substantial decrease in NO_2 concentrations over North America in the past decade [*Kharol et al.*, 2015; *Krotkov et al.*, 2016]. On the contrary, NH_3 concentrations have increased over most of North America and other major agricultural regions of the world [*Warner et al.*, 2017], and are expected to continue to rise in the future with increasing demands on more and better food production to supply a growing global population [*Bauer et al.*, 2016; *Reis et al*., 2009]. For example, *Paulot et al*. [2013] using future International Panel on Climate Change (IPCC) representative concentration pathways (RCPs) scenarios for 2010−2050 [*Lamarque et al.*, 2011**;** *van Vuuren et al.*, 2011] showed that future decreases in N_r deposition due to NO_x emission controls will be offset by concurrent increases in ammonia emissions from agriculture. *Ellis et al.* [2013] also found using the same IPCC RCP scenarios that by 2050 ammonia will dominate nitrogen deposition in the US. In addition to these ecosystem impacts, any future changes in N_r deposition will also have climate impacts, for example, changes are likely to induce a negative climate forcing by increasing carbon sinks (increased plant growth and thus their uptake of CO_2) [*Reay et al.*, 2008]. Considering all of these aspects there is an immediate and growing need to better understand and quantify present day dry deposition of reactive nitrogen, including from NH_3 and NO_2 (represented here by N_r^p, where p is the contribution of NH_3 and NO_2 to the total reactive nitrogen), regionally and globally.

Surface in-situ measurement networks for N_r concentration measurements and deposition estimates are sparse and lack the necessary spatial coverage, especially in remote regions and developing countries. Until recently the goal of providing spatially-resolved N_r deposition has been accomplished only with the use of numerical modelling [*Zhang et al.*, 2012; *Paulot et al.*, 2013; *Lee et al.*, 2016]. However, satellite-based instruments can play a large role in fulfilling this goal with their ability to provide (near) global daily coverage. While there are many reactive nitrogen compounds in the ecosystem, at present satellites sensors are only able to provide

information on the near-surface concentration of two: nitrogen dioxide (NO_2) [e.g., *Kharol et al., 2015*] and ammonia (NH_3) [e.g., *Shephard et al., 2011*]. Fortunately, these two chemical species represent a significant fraction of N_r dry deposition overall, particularly the component that displays high spatial variability and, together with nitric oxide (NO), make up approximately 90% of the total N_r emitted that is deposited back to the surface [*Galloway et al.*, 2004].

Previous studies have used space-based measurements of NO_2 for estimating deposition [*Nowlan et al., 2014; Jia et al., 2016; Geddes et al., 2017*], but this study is the first to directly use satellite observations of both NH_3 and NO_2 to derive dry deposition fluxes and their relative importance. Also presented are insights on the impact of forest fires in the dry deposition of N_r^p from NH_3 over northern latitudes, where there is little contribution from agricultural sources.

2. Materials and Methods

2.1 Cross-track Infrared Sounder (CrIS) Satellite

CrIS was launched in late October 2011 on board the Suomi National Polar-orbiting Partnership (SNPP) platform. SNPP follows a sun-synchronous orbit with a daytime overpass time at 13:30 local solar time and a night time overpass at 01:30. The instrument scans along a 2200 km swath using a 3 x 3 array of circular pixels with a diameter of 14 km at nadir for each pixel. The 970 cm^{-1} spectral region used in the ammonia retrievals has a spectral resolution of 0.625 cm^{-1} (unapodized) with an excellent spectral noise of ~0.05K@270K [*Zavyalov et al.*, 2013]. The CrIS Fast Physical Retrieval (CFPR) described by *Shephard and Cady-Pereira* [2015] is an optimal estimation approach [*Rodgers*, 2000] used to perform satellite profile retrievals of ammonia volume mixing ratio (VMR), and builds on the heritage of the Tropospheric Emission Spectrometer (TES) ammonia retrieval [*Shephard et al.*, 2011]. Following *Shephard et al.* [2011], the retrieval uses three different a priori ammonia profiles representing unpolluted, moderate, and polluted conditions as the prior knowledge of ammonia is poorly known over the entire globe (which is required for a global retrieval). In addition to the VMR profile, the retrieval also provides the satellite vertical sensitivity (averaging kernels) and an estimate of the total errors (error covariance matrix). This is important as the satellite sensitivity and vertical resolution varies from profile-to-profile depending on the atmospheric state (i.e., thermal profile, ammonia concentrations, cloud cover, etc.). For a typical retrieved profile the sensitivity directly at the surface can be limited [*Shephard and Cady-Pereira*, 2015], with broad vertical resolution (~1-km). Thus, even though the retrieval is performed at independent levels through the atmospheric profile, the retrieved surface level values are generally correlated with the retrieval boundary level values above it in the ~1-3 km vertical range. The detectability limit of CrIS surface NH_3 is ~0.5 ppbv under favourable conditions. Initial CrIS validation studies show that CrIS compares well with ground-based Fourier Transform Infrared (FTIR) [*Dammers et al.*, 2017] measurements with a correlation of 0.77, and very little bias (+2%) in the total column values. The profile comparisons show that the CrIS and the FTIR single profile level differences are typically between 20 to 40%, which are within the range of the CrIS estimated retrieval errors provided with the product.

2.2 Ozone Monitoring Instrument (OMI)

OMI is a nadir-viewing, UV-visible spectrometer on board on the Aura satellite, launched in July 2004 [*Levelt et al*., 2006]. Aura is also in a sun-synchronous orbit with an overpass time of 13:30 although differences in observation time with SNPP can be as much as an hour over North America. OMI provides near-daily global coverage of NO_2 with a variable ground spatial resolution of 13 km × 24 km at nadir to 140 km × 26 km at swath edge. We use the OMI operational NO_2 standard product (SP), version-3 [*Krotkov and Veefkind, 2016; Krotkov et al.,* 2017] (https://disc.gsfc.nasa.gov/datasets/OMNO2_V003/summary).

Surface concentrations of NO_2 were derived from the SP in a two-step process that utilizes output from the Environment and Climate Change Canada GEM-MACH (Global Environmental Multi-scale - Modelling Air quality and Chemistry) regional air quality model [*Gong et al.,* 2015]. GEM refers to the operational meteorological forecast model, and MACH to the chemical package. First, the sensitivity of OMI to an individual scene, as quantified by a so-called air mass factor (AMF), is recalculated using NO_2 profiles from GEM-MACH (at 15 km x 15 km) along with some other high resolution input information [*McLinden et al.*, 2014; 2016]. Second, the same GEM-MACH profiles are used to convert the tropospheric vertical column density of NO_2 to surface volume mixing ratios following the general approach described by *Lamsal et al.* [2008] and also used in *McLinden et al.* [2014]. While individual NO_2 observations can have random errors in excess of $>10^{15}$ molecules/cm^2 in the column, their effect should be minimal in an annual average. A modest 15% low bias in OMI-derived NO_2 surface concentrations was found over the oil sands once spatial resolution was accounted for [*McLinden et al.,* 2014]. Comparisons with surface monitoring sites across the rest of Canada and the US suggest even smaller low biases, on average ~6%.

One additional consideration is that the NO_2 product used here does not properly account for forest fires. Fire plumes can contain large amounts of NO_2, leading to a substantially different profile shape than predicted by the model, and aerosol in the plume will modify the light path. While their overall impact is complex and depends on plume height, details of the aerosol, and other factors, ignoring these effects will likely lead to an underestimate of NO_2 in the plume [*Bousserez,* 2014]. This, in turn, will bias the NO_2 flux low in regions prone to fires.

2.3 Dry deposition flux calculation

To estimate dry deposition fluxes, satellite observations of surface NH_3 and NO_2 ($\boldsymbol{C}$) are combined with modeled unidirectional dry deposition velocities ($\boldsymbol{V_d}$) [*Zhang et al.,* 2003]. The dry deposition flux ($\boldsymbol{F_d}$) can be defined as:

$$\boldsymbol{F_d} = -\boldsymbol{V_d} \times \boldsymbol{C} \qquad (1)$$

The deposition velocity is a function of the surface type and properties and meteorological parameters, the latter of which are taken from GEM model. We use MODIS (MODerate Resolution Imaging Spectrometer) satellite derived land-use / land-cover types (MCD12Q1, https://lpdaac.usgs.gov/dataset_discovery/modis/modis_products_table/mcd12q1) and archived 8-day average leaf area index (LAI) (MCD15A2,

https://lpdaac.usgs.gov/dataset_discovery/modis/modis_products_table/mcd15a2) at 0.5 km x 0.5 km and 1 km x 1 km spatial resolution respectively. Both land-use / land-cover types and LAI were regridded to that of GEM at 15 km x 15km.

To convert the NO_2 dry deposition flux to a daily average, we followed the method developed by *Nowlan et al.* [2014] and calculated the 24-h daily flux $\boldsymbol{F^{sat}}$, as follows:

$$\boldsymbol{F^{sat}} = -(\overline{\boldsymbol{V_d}} \times \boldsymbol{C^{sat}}) \times \frac{\boldsymbol{C_{24}^{GM}}}{\boldsymbol{C_{13-15}^{GM}}} \quad (2)$$

Where $\overline{\boldsymbol{V_d}}$ represents daily mean dry deposition velocity, $\boldsymbol{C^{sat}}$ represents the satellite-derived ground-level concentration, $\boldsymbol{C_{24}^{GM}}$ and $\boldsymbol{C_{13-15}^{GM}}$ represents 24-h and satellite overpass time mean ground-level concentrations from GEM-MACH model. For NH_3 we assumed the mid-day deposition flux to be similar to the diurnal average [e.g. *Phillips et al.*, 2006] so no adjustments were made.

3. Results and Discussion

The ground-level satellite concentrations and the corresponding dry deposition fluxes of NH_3 and NO_2 are shown in Figure 1 for the 2013 North American warm season (April-September). For ease of reference, the corresponding N_r^p dry deposition fluxes in Figure 1 are also converted to total warm season deposition amounts in supplementary Figure S1. Note the domain in the figures matches that of GEM-MACH, the source of NO_2 profiles, which excludes Mexico and the southernmost portion of Texas. It can be seen from Figure 1a that the elevated (over 3 ppbv) NH_3 regions generally coincide with agricultural regions across North America. There are larger "hot spots" in the US with means over 10 ppbv that include the Central Valley in California, portions of Idaho and Washington State, and several states in the central US (e.g., Nebraska, Kansas, Oklahoma, Northern Texas). The peaks for Canadian agriculture regions tend to be smaller, with values in the range of ~3 to 5 ppbv (e.g., Lethbridge, Alberta; Winnipeg, Manitoba; Southwestern Ontario; Le Centre-du-Quebec Region). Hotspots over northern Canada are mainly associated with forest fire emissions (additional details provided below) where, despite their episodic nature, emissions are large enough to ensure elevated concentrations even when averaged over the entire warm season and with monthly mean values reaching ~8 ppbv (not shown). The spatial distribution of the NH_3 dry deposition flux (Figure 1d) largely follows the NH_3 concentrations (Figure 1a), including hotspot location, but tends to be muted in most of the western US, reflecting the lower dry deposition velocities in that region. Figure 1d shows 2013 warm season average NH_3 deposition fluxes exceed 125 μg N m^{-2} hr^{-1} over central California and the core of the US Midwest. Figure S2 shows the intermonthly variation in the NH_3 dry deposition of N_r^p over the warm season, which captures the expected increase in NH_3 dry deposition from increased fertilizer applications starting in April in the US and May in Canada, with many regions having fluxes greater than 125 μg N m^{-2} hr^{-1} in a given month. The similarity in spatial patterns of concentrations and deposition flux are expected given that NH_3 reacts quickly in the atmosphere with a lifetime of several hours to a day. Thus, high concentrations and dry deposition fluxes will generally occur in emission areas [*Hertel et al.*, 2012; *Zhang et al.*, 2009] suggesting the impacts of NH_3 on ecosystems are higher near source regions.

The corresponding map of NO_2 concentrations over North America in Figure 1b and Figure S3, shown at OMI local time, reveal hotspots that are mainly located over urban and industrial regions. In the US, the highest density of hotspots occurs in the east, with localized concentrations over 10 ppbv, whereas for Canada the hotspots are mostly in the large urban regions of southern Ontario and Quebec (e.g., the Greater Toronto Area (GTA) with peak values of over 10 ppbv), and over the oil and gas source regions of Alberta, with elevated values in the range of 3-7 ppbv. NO_2 is also a short-lived atmospheric species (≤1 day lifetime) and so the general spatial pattern of dry deposition of NO_2 across North America (Figure 1e), based on diurnally averaged NO_2 (see Eq. 2), is similar to the NO_2 concentration map (Figure 1b). Dry deposition fluxes generally exceed 35 μg N m^{-2} hr^{-1}, over larger urban and industrial locations with some hotspots reaching over 125 μg N m^{-2} hr^{-1}. Similar wide-spread elevated flux values appear in Alberta, Canada. The intermonthly variation over the warm season for NO_2 (refer to Figure S3) is not as large as it is for NH_3, which has a strong dependence on the timing of agriculture fertilizer applications.

The combined ground level N_r^p concentrations and dry deposition fluxes of both NH_3 and NO_2 are plotted in Figure 1c and Figure 1f and, as expected, indicate that dry deposition is highest in the agriculture regions (mostly from NH_3) and more localized urban and industrial regions (mostly from NO_2). The relative NH_3 and NO_2 contributions to the dry deposition of N_r^p across North America, shown in Figure 1, are plotted as a ratio [NO_2/(NH_3+NO_2)] in Figure 2: yellow and red areas (>0.5) have a greater contribution of dry deposition from NO_2 deposition, whereas the darker blue values (<0.5) indicate a greater contribution from NH_3. Figure 2a shows the spatially resolved ratios, while Figure 2b shows the ratio averaged over the geopolitical boundaries (provinces, territories, and states) across North America. The average fluxes and the ratios for the geopolitical boundaries, ordered from NH_3 to NO_2 dominance, are also provided in Table S1. Integrating the flux over space and the warm season, ammonia tends to dominate N_r^p deposition, contributing ~80%, or a 4:1 NH_3:NO_2 ratio, in Canada, and ~65% (2:1) in the US. In fire prone regions, the NO_2 contribution should be considered more of a lower limit due to the current limitation in the NO_2 retrieval. Furthermore, some seasonality is expected in this ratio at higher latitudes due to reduced NH_3 emission (no fertilizer applications and lower temperatures) and slower photochemical removal of NO_x in the winter months leading to higher ratios. Nevertheless, these results indicate that for the majority of the geopolitical regions in Canada and the US the dry deposition of NH_3 exceeds that of NO_2 and considering the expected trends in NH_3 and NO_2 emissions, this preponderance is only expected to increase.

In the US over the 2013 warm season, ~53 tonnes (N) of N_r^p were deposited, more than double the ~23 tonnes (N) for Canada. As shown in both Figure 2 and Table S1, 43 out of the 50 US states indicate more dry deposition from NH_3 compared with NO_2, with the agricultural states of South Dakota, Nebraska, and Kansas exceeding 80% and peaks fluxes of ~70 μg N m^{-2} hr^{-1}. The only exceptions are states in the northeastern US which favor NO_2.

Examining the link between forest fire activity and NH_3, total MODIS fire counts for the 2013 warm season are plotted in Figure 3a and Figure 3b for two large regions of Northern Canada (see supplementary Figure S5). The corresponding NH_3 dry deposition fluxes are shown in panels (c) and (d) of Figure 3 (the same as shown in Figure 1b). To provide insight on the relative contributions of forest fires to the dry deposition of N_r^p from NH_3 in these northern

regions, we estimated the dry deposition flux of N_r^p from NH_3 without fires by assuming a constant warm season background satellite derived NH_3 value of 1.0 ppbv with the same dry deposition velocities. This background value is based on representative background satellite values over this region during this period. These estimated background fluxes are shown in panels (e) and (f) of Figure 3. The ratio of the total observed to estimated background flux (Figure 3 panels (g) and (h)) suggest that over these regions the N_r^p dry deposition flux from NH_3 is 2-3 times larger than typical background amounts.

Evaluating the dry deposition fluxes, including those presented here, remains a large challenge. Direct measurements of NH_3 and NO_2 fluxes are very rare, expensive and technically challenging [*Nowlan et al.,* 2014; *Zhang et al.,* 2010]. Without these, such evaluations amount to a comparison of two estimates in which each is a product of two quantities: surface concentration and deposition velocity. Deposition velocity schemes are highly parameterized and can give widely different results [e.g., *Schwede et al.,* 2011]. If the same velocity scheme is used then flux comparisons amount to a comparison of surface concentrations. The National Atmospheric Deposition Program (NADP) computes the dry deposition flux of nitrogen using a "hybrid approach" involving surface monitoring and the Community Multiscale Air Quality (CMAQ) model to fill spatial gaps and nitrogen species not observed in the network (e.g., NO_2) [*Schwede and Lear,* 2014]. Qualitative comparisons with NADP NH_3 dry deposition annual fluxes [NADP, 2017], which utilizes a different deposition velocity scheme, with our warm-season results reveal a general consistency in both the spatial distribution and absolute values for the US (refer to Figure S1) when the seasonality of emissions from regions dominated by livestock or multi growing seasons are considered. Another recent study by *Jia et al.* [2016] shows spatial maps of the annual dry deposition of NO_2 (from OMI) and NH_3 (at surface station locations). Again our dry deposition results are in general agreement in terms of spatial pattern and magnitude, with NO_2 dry deposition ranging in North America from ~0.1 to 2.0 kg N ha^{-1} yr^{-1}, and the NH_3 values ranging from ~0.5 to 10 kg N ha^{-1} yr^{-1}, which are comparable to our values in Figure S1, especially considering the different durations. *Phillips et al.* [2006] showed, for the summer 1999, averaged dry deposition fluxes of ~15 and ~34 µg N m^{-2} hr^{-1} for NO_2 and NH_3 in North Carolina respectively, which are in a similar range to our satellite-derived fluxes of ~17 and ~27 µg N m^{-2} hr^{-1} for NO_2 and NH_3 in North Carolina during the 2013 warm season as shown in Table S1.

4 Conclusions

Due to various negative impacts of excess N_r on sensitive ecosystems there is a significant need for observational-based estimates of N_r dry deposition fluxes, particularly in regions without sufficient surface monitoring. Towards that end, this analysis provides a first look at the magnitudes and relative importance of N_r^p NH_3 and NO_2 dry deposition across North America based on satellite observations. As expected for these short-lived chemical species, the hot-spots of N_r^p dry deposition typically occur close to emission sources where concentrations are largest, near urban and industrial sources for NO_2 and agricultural sources for NH_3. Nationwide, for the 2013 warm season, ~53 tonnes (N) were dry deposited in the US and ~23 tonnes (N) in Canada with NH_3 accounting for about 65% in the US and 80% in Canada of total N_r^p. In terms of spatial distribution, the NH_3 dry deposition flux exceeds that of NO_2, with the exception of a small number of states largely located in the northeastern US. In Canada, Alberta is the only province

with roughly equal fluxes of NH_3 and NO_2, which is likely due to additional NO_2 contributions from the oil and gas sector. We also show that forest fires are the major contributors of NH_3 dry deposition in northern latitudes during the warm season where they often deposit 2-3 times more N_r^p from NH_3 than similar areas not affected by forest fire emissions.

Bauer et al. [2016] reported that half of the total anthropogenic pollution in the US is mainly due to agricultural practices. With ambient NO_x concentrations decreasing across most of North America due to emission regulations and controls, and with NH_3 currently increasing and predicted to continue to do so, balancing the deposition of N_r into the ecosystem (for such needs as food production) with the potential ecosystem impacts from excess nitrogen, requires enhanced monitoring observations of N_r. The spatial mapping of N_r^p dry deposition fluxes derived from satellite observations of NH_3 and NO_2 over North America provided here can be used to help make informed decisions on mitigation strategies for environmental protection. In the future we will extend this analysis to include the full CrIS observational period in order to investigate seasonal and interannual variability and trends, and refine the OMI NO_2 retrievals over biomass burning areas.

Acknowledgments

We would like to thank Paul Makar, J. Zhang**,** and Amanda Cole at ECCC for their helpful discussions. SKK was supported through the Natural Sciences and Engineering Research Council of Canada Visiting Fellowship program. We would like to acknowledge the University of Wisconsin-Madison Space Science and Engineering Center Atmosphere SIPS team sponsored under NASA contract NNG15HZ38C for providing us with the CrIS level 1 input data, in particular Kevin Hrpcek and Liam Gumley. The level 2 CrIS NUCAPS input data (e.g. temperature, water vapour profiles, etc.) were obtained from the NOAA Comprehensive Large Array-Data Stewardship System (CLASS) [*Liu et al.,* 2014], with special thanks to Axel Graumann (NOAA) for helping with the downloads. We would also like to thank Andre Wehe (AER) for initial development of the CrIS download and extraction software for the retrieval inputs. This work was also funded at AER through a NASA (contract: NNH15CM65C). The data used in this study can be made available on request (Shailesh K. Kharol and Chris A. McLinden, Environment and Climate Change Canada, Toronto, Ontario, Canada).

References

Bauer, S. E., K. Tsigaridis, and R. Miller (2016), Significant atmospheric aerosol pollution caused by world food cultivation, Geophys. Res. Lett., 43, 5394-5400, doi:10.1002/2016GL068354.

Bergstrom, A. –K., and M. Jansson (2006), Atmospheric nitrogen deposition has caused nitrogen enrichment and eutrophication of lakes in the northern hemisphere, Global Change Biology, 12, 635-643, doi:10.1111/j.1365-2486.2006.01129.x.

Bousserez, N. (2014), Space-based retrieval of NO_2 over biomass burning regions: quantifying and reducing uncertainties, Atmos. Meas. Tech., 7, 3431-3444, https://doi.org/10.5194/amt-7-3431-2014.

348 Bowman, W. D., J. Murgel, T. Blett, and E. Porter (2012), Nitrogen critical loads for alpine
349 vegetation and soils in Rocky Mountain National Park, J. Environ. Manage., 103, 165–
350 171, doi:10.1016/j.jenvman.2012.03.002, 2012.

351 Dammers, E., M. W. Shephard, M. Palm, K. E. Cady-Pereira, S. Capps, E. Lutsch, K. Strong, J.
352 W. Hannigan, G. C. Toon, W. Stremme, M. Grutter, N. Jones, D. Smale, J. J. Siemons,
353 K. Hrpcek, D. Tremblay, M. Schaap, J. Notholt, J. W. Erisman, (2017), Validation of the
354 CrIS fast physical NH3 retrieval with ground-based FTIR, Atmos. Meas. Tech. Discuss.,
355 doi:10.5194/amt-2017-38, 2017.

356 Ellis, R. A., D. J. Jacob, M. P. Sulprizio, L. Zhang, C. D. Holmes, B. A. Schichtel, T. Blett, E.
357 Porter, L. H. Pardo, and J. A. Lynch (2013), Present and future nitrogen deposition to
358 national parks in the United States: critical load exceedances, Atmos. Chem. Phys., 13,
359 9083-9095, doi:10.5194/acp-13-9083-2013.

360 Erisman, J. W., J. Galloway, S. Seitzinger, A. Bleeker, and K. Butterbach-Bahl (2011), Reactive
361 nitrogen in the environment and its effect on climate change, Current Opinion in
362 Environmental Sustainability, 3, 281-290.

363 Erisman, J. W., J. N. Galloway, N. B. Dice, M. A. Sutton, A. Bleeker, B. Grizzetti, A. M. Leach,
364 and W. de Vries (2015), Nitrogen: too much of a vital resource. Science Brief. WWF
365 Netherlands, Zeist, The Netherlands.

366 Fenn, M. E., E. B. Allen, S. B. Weiss, S. Jovan, L. H. Geiser, G. S. Tonnesen, R. F. Johnson, L.
367 E. Rao, B. S. Gimeno, F. Yuan, T. Meixner, and A. Bytnerowicz (2010), Nitrogen critical
368 loads and management alternatives for N-impacted ecosystems in California, J. Environ.
369 Manage., 91, 2404–2423, doi:10.1016/j.jenvman.2010.07.034, 2010.

370 Fowler, D., et al. (2013), The global nitrogen cycle in the twenty-first century, Philos. Trans. R.
371 Soc. B, 368, 20130164, doi:10.1098/rstb.2013.0164.

372 Fowler, D., et al. (2015), Effects of global change during the 21st century on the nitrogen cycle,
373 Atmos. Chem. Phys., 15, 13,849-13,893, doi:10.5194/acp-15-13849-2015.

374 Galloway, J. N., J. D. Aber, J. W. Erisman, S. P. Seitzinger, R. W. Howarth, E. B. Cowling, and
375 B. J. Cosby (2003), The nitrogen cascade, Bioscience, 53, 341–356.

376 Galloway, J. N., et al. (2004), Nitrogen cycles: past, present, and future, Biogeochemistry, 70,
377 153-226.

378 Geddes, J. A. and Martin, R. V. (2017), Global deposition of total reactive nitrogen oxides from
379 1996 to 2014 constrained with satellite observations of NO_2 columns, Atmos. Chem.
380 Phys. Discuss., https://doi.org/10.5194/acp-2016-1100, in review.

381 Gong,W., P. A. Makar, J. Zhang, J. Milbrandt, S. Gravel, K. L. Hayden, A. M. Macdonald, and
382 W. R. Leaith (2015), Modelling aerosolcloud-meteorology interaction: a case study with
383 a fully coupled air quality model (GEM-MACH), Atmos. Environ., 115, 695–715.

384 Hertel, O., et al. (2012), Governing processes for reactive nitrogen compounds in the European
385 atmosphere, Biogeosciences, 9, 4921-4954.

386 Jia, Y., G. Yu, Y. Gao, N. He, Q. Wang, C. Jiao and Y. Zuo (2016), Global inorganic nitrogen
387 dry deposition inferred from ground- and space-based measurements. Sci. Rep., **6**, 19810;
388 doi: 10.1038/srep19810.

Kharol, S. K., R. V. Martin, S. Philip, B. Boys, L. N. Lamsal, M. Jerrett, M. Brauer, D. L. Crouse, C. McLinden, and R. T. Burnett (2015), Assessment of the magnitude and recent trends in satellite-derived ground-level nitrogen dioxide over North America, Atmos. Environ., 118, 236–245.

Krotkov, N. A., C. A. McLinden, C. Li, L. N. Lamsal, E. A. Celarier, S. V. Marchenko, W. H. Swartz, E. J. Bucsela, J. Joiner, B. N. Duncan, K. F. Boersma, J. P. Veefkind, P. F. Levelt, V. E. Fioletov, R. R. Dickerson, H. He, Z. Lu, and D. G. Streets (2016), Aura OMI observations of regional SO_2 and NO_2 pollution changes from 2005 to 2015, Atmos. Chem. Phys., 16, 4605– 4629, doi:10.5194/acp-16-4605-2016.

Krotkov, N. A. and P. Veefkind (2016), OMI/Aura Nitrogen Dioxide (NO_2) Total and Tropospheric Column 1-orbit L2 Swath 13x24 km V003, Greenbelt, MD, USA, Goddard Earth Sciences Data and Information Services Center (GES DISC), Accessed [*January 2017*], DOI:10.5067/Aura/OMI/DATA2017.

Krotkov, N. A., Lamsal, L. N., Celarier, E. A., Swartz, W. H., Marchenko, S. V., Bucsela, E. J., Chan, K. L., and Wenig, M.: The version 3 OMI NO2 standard product, Atmos. Meas. Tech. Discuss., https://doi.org/10.5194/amt-2017-44, in review, 2017.

Lamarque, J. –F., G. P. Kyle, M. Meinshausen, K. Riahi, S. J. Smith, D. P. van Vuuren, A. J. Conley, and F. Vitt (2011), Global and regional evolution of short-lived radiatively-active gases and aerosols in the representative concentration pathways, Climate Change, 109, 191-212, doi:10.1007/s10584-011-0155-0.

Lamsal, L. N., R. V. Martin, A. van Donkelaar, M. Steinbacher, E. A. Celarier, E. Bucsela, E. J. Dunlea, and J. P. Pinto (2008), Ground-level nitrogen dioxide concentrations inferred from the satellite-borne Ozone Monitoring Instrument, J. Geophys. Res., 113, D16308, doi:10.1029/2007JD009235.

Lee, H.-M., F. Paulot, D. K. Henze, K. Travis, D. J. Jacob, L. H. Pardo, and B. A. Schichtel (2016), Sources of nitrogen deposition in Federal Class I areas in the US, Atmos. Chem. Phys., 16, 525-540, https://doi.org/10.5194/acp-16-525-2016.

Levelt, P. F., G. H. J. van den Oord, M. R. Dobber, A. Malkki, H. Visser, J. de Vries, P. Stammes, J. O. V. Lundell, and H. Saari (2006), The Ozone Monitoring Instrument, IEEE T. Geosci. Remote, 44, 1093–1101.

Liu, Q., W. Wolf, T. Reale, A. Sharma, and NOAA JPSS Program Office (2014), NESDIS-Unique CrIS-ATMS Product System (NUCAPS) Environmental Data Record (EDR) Products. NOAA National Centers for Environmental Information. doi:10.7289/V52F7KG5 [Last accessed on 14/07/2017] https://doi.org/10.7289/V52F7KG5.

McLinden, C, A., V. E. Fioletov, K. F. Boersma, S. K. Kharol, N. A. Krotkov, L. Lamsal, P. A. Makar, R. V. Martin, J. P. Veefkind, and K. Yang (2014), Improved satellite retrievals of NO_2 and SO_2 over the Canadian oil sands and comparisons with surface measurements, Atmos. Chem. Phys., 14, 3637-3656.

McLinden, C. A., V. Fioletov, N. Krotkov, C. Li, K. F. Boersma, and C. Adams (2016), A decade of change in NO_2 and SO_2 over the Canadian oil sands as seen from space, Env. Sci. Tech., 50(1), 331-337, doi:10.1021/acs.est.5b04985.

NADP, 2017, National Atmospheric Deposition Program (NRSP-3), Available from the NADP Program Office, Illinois State Water Survey, 2204 Griffith Dr., Champaign, IL, USA, http://nadp.isws.illinois.edu.

Nowlan, C. R., R. V.Martin, S. Philip, L. N. Lamsal, N. A. Krotkov, E. A. Marais, S. Wang, and Q. Zhang (2014), Global dry deposition of nitrogen dioxide and sulfur dioxide inferred from space-based measurements, *Global Biogeochem. Cycles, 28,* doi:10.1002/2014GB004805.

Paulot, F., D. J. Jacob, and D. K. Henze (2013), Sources and processes contributing to nitrogen deposition: an adjoint model analysis applied to biodiversity hotspots worldwide, Environ. Sci. Technol., 47, 3226-3233.

Phillips, S. B., V. P. Aneja, D. Kang, and S. P. Arya (2006), Modelling and analysis of the atmospheric nitrogen deposition in North Carolina, Int. J. of Global Environmental Issues, Vol. 6, No. 2/3, 231-252.

Reay D.S, F. Dentener, P. Smith, J. Grace, and R.A. Feely (2008), Global nitrogen deposition and carbon sinks. Nat Geosci., 1, 430–437, doi:10.1038/Ngeo230, 2008.

Reis, S., R. W. Pinder, M. Zhang, G. Lijie, and M. A. Sutton (2009), Reactive nitrogen in atmospheric emission inventories, Atmos. Chem. Phys., 9, 7657-7677, doi:10.5194/acp-9-7657-2009.

Rodgers, C. D. (2000), Inverse methods for atmospheric Sounding: Theory and Practice, World Sci., Hackensack, NJ, 2000.

Schwede, D., L. Zhang, R. Vet, and G. Lear (2011), An intercomparison of the deposition models used in the CASTNET and CAPMoN networks, Atmos. Environ., 45, 1337-1346, doi:10.1016/j.atmosenv.2010.11.050.

Shephard M.W., K. E. Cady-Pereira, M. Luo, D. K. Henze, R. W. Pinder, J. T. Walker, C. P. Rinsland, J. O. Bash, V. Payne, L. Clarisse (2011), TES ammonia retrieval strategy and global observations of the spatial and seasonal variability of ammonia, Atmos. Chem. Phys., 11, 10743-10763, doi:10.5194/acp-11-10743-2011.

Shephard, M. W., and K. E. Cady-Pereira (2015), Cross-track Infrared Sounder (CrIS) satellite observations of tropospheric ammonia, Atmos. Meas. Tech., 8, 1323–1336, doi:10.5194/amt-8-1323-2015.

Sheppard, L. J., I. D. Leith, T. Mizunuma, J. N. Cape, A. Crossley, S. Leeson, M. A. Sutton, N. van Dijk, and D. Fowler (2011), Dry deposition of ammonia gas drives species change faster than wet deposition of ammonium ions: evidence from a long-term field manipulation, Global Change Biology, 17, 3589-3607, doi:10.1111/j.1365-2486.2011.02478.x.

Schwede, D.B., and G.G. Lear (2014), A novel hybrid approach for estimating total deposition in the United States, Atmospheric Environment, 92, 207-220, doi:dx.doi.org/10.1016/j. atmosenv.2014.04.008.

van Vuuren, D. P., J. Edmonds, M. Kainuma, K. Riahi, A. Thomson, K. Hibbard, G. C. Hurtt, T. Kram, V. Krey, J. F. Lamarque, T. Masui, M. Meinshausen, N. Nakicenovic, S. J. Smith,

and S. K. Rose (2011), The representative concentration pathways: an overview, Climatic Change, 109, 5–31, doi:10.1007/S10584-011-0148-Z, 2011.

Warner, J. X., R. R. Dickerson, Z. Wei, L. L. Strow, Y. Wang, and Q. Liang (2017), Increased atmospheric ammonia over the world's major agricultural areas detected from space, Geophys. Res. Lett., 44, doi:10.1002/2016GL072305.

Zavyalov, V., M. Esplin, D. Scott, B. Esplin, G. Bingham, E. Hoffman, C. Lietzke, J. Predina, R. Frain, L. Suwinski, Y. Han, C. Major, B. Graham, and L. Phillips (2013), Noise performance of the CrIS instrument, J. of Geophysical Research, 118, 13,108–13,120, doi:10.1002/2013JD020457, 2013.

Zhang, L., J. R. Brook, and R. Vet (2003), A revised parameterization for gaseous dry deposition in air-quality models, Atmos.Chem. Phys., 3, 2067-2082.

Zhang, L., R. Vet, J. M. O'Brien, C. Mihele, Z. Liang, and A. Wiebe (2009), Dry deposition of individual nitrogen species at eight Canadian rural sites, J. Geophys. Res., 114, D02301, doi:10.1029/2008JD010640.

Zhang, L., L. P. Wright, and W. A. H. Asman (2010), Bi-directional air-surface exchange of atmospheric ammonia: A review of measurements and a development of a big-leaf model for applications in regional-scale air-quality models, J. Geophys. Res., 115, D20310, doi:10.1029/2009JD013589.

Zhang, L., D. J. Jacob, E. M. Knipping, N. Kumar, J. W. Munger, C. C. Carouge, A. van Donkelaar, Y. X. Wang, and D. Chen (2012), Nitrogen deposition to the United States: distribution, sources, and processes, Atmos. Chem. Phys., 12, 4539–4554, doi:10.5194/acp-12-4539-2012.

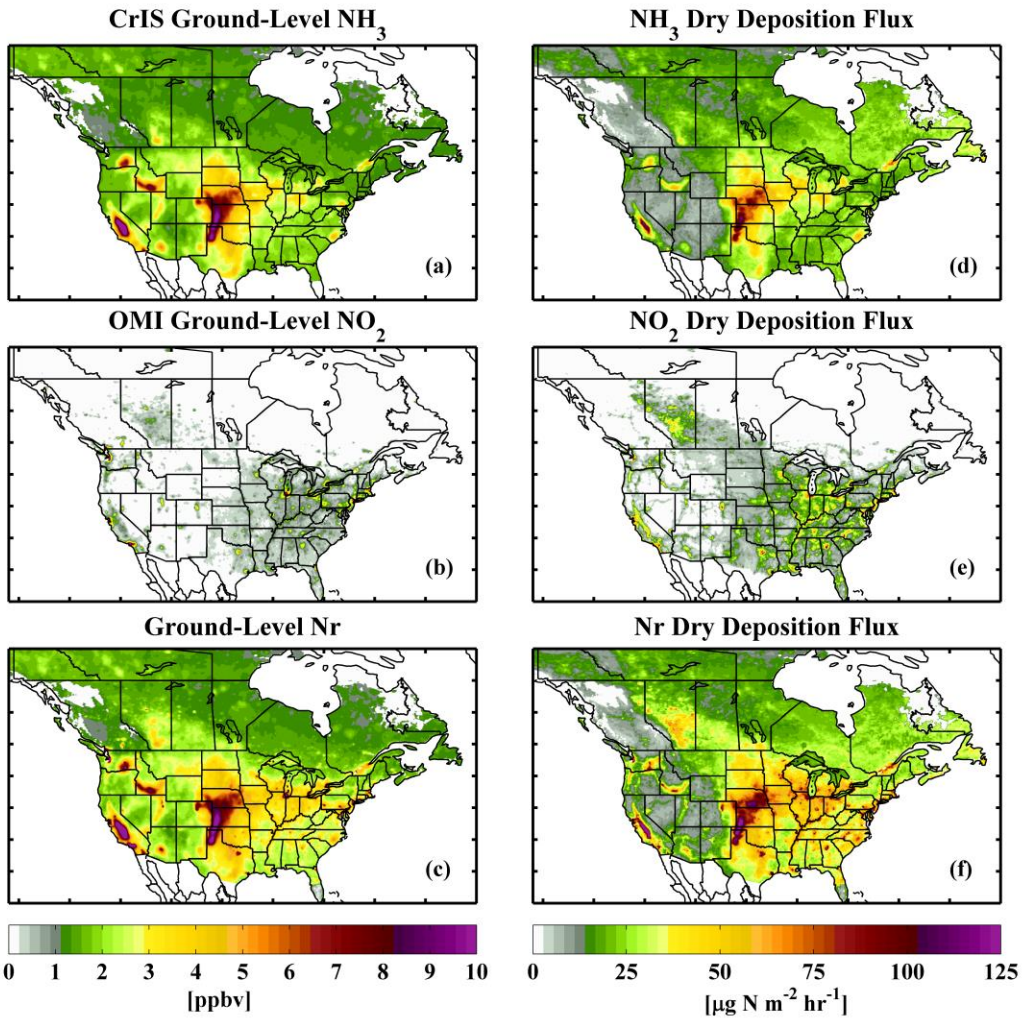

Figure 1. Satellite-derived warm season mean ground-level concentrations and dry deposition fluxes of NH_3, NO_2, and N_r (NH_3 + NO_2) over North America.

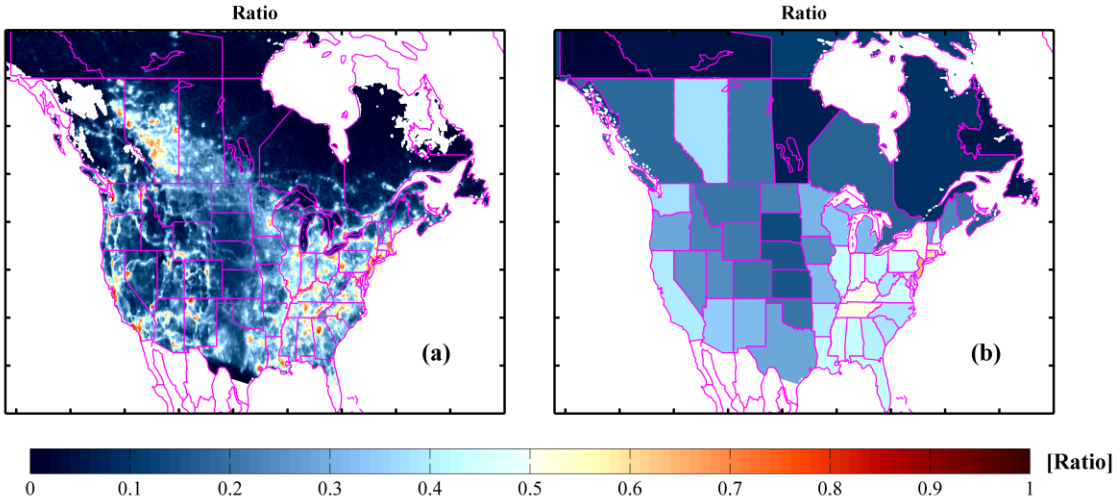

498
499

Figure 2. Ratio of nitrogen dioxide (NO_2) to Total N_r (NH_3+NO_2) dry deposition flux over North America. The yellow-to- red (values >0.5) areas indicate where the dry deposition of N_r (NH_3+NO_2) has a greater contribution from NO_2, whereas the blue (values <0.5) regions indicate dominant NH_3 dry deposition.

500

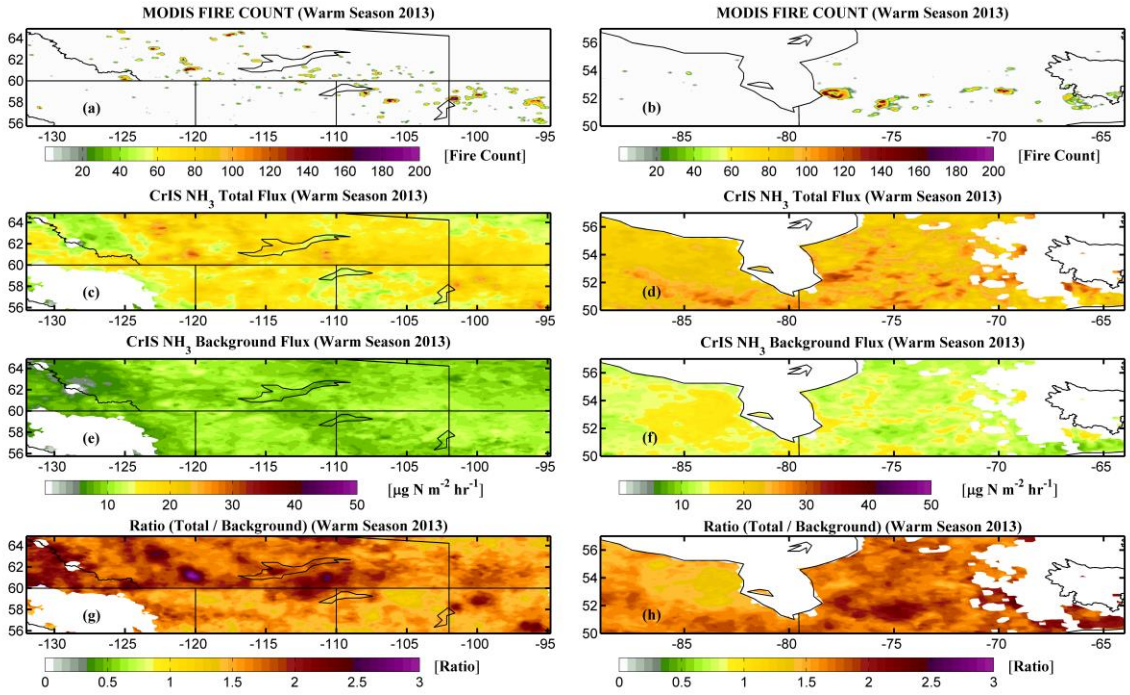

501

Figure 3. Warm season (April-September, 2013) MODIS Fire Count (a,b), CrIS NH_3 total dry deposition flux (c,d), CrIS NH_3 background dry deposition flux (e,f), and flux ratio (g,h) over the two northern regions of Canada.